A combination of the acoustic radiosity and the image source method

Koutsouris, Georgios I. ; Brunskog, Jonas; Jeong, Cheol-Ho; Jacobsen, Finn

Published in:
Internoise 2012

Publication date:
2012

Document Version
Publisher's PDF, also known as Version of record

A combination of the acoustic radiosity and the image source method

Georgios I. Koutsouris[1]
Jonas Brunskog[2]
Cheol-Ho Jeong[3]
Finn Jacobsen[4]
Acoustic Technology, DTU Electro, Technical University of Denmark, Kongens Lyngby DK-2800, Denmark

A combined model for room acoustic predictions is developed, aiming to treat both diffuse and specular reflections in a unified way. Two established methods are incorporated: acoustical radiosity, accounting for the diffuse part, and the image source method, accounting for the specular part. The model is based on conservation of acoustical energy. Losses are taken into account by the energy absorption coefficient, and the diffuse reflections are controlled via the scattering coefficient, which defines the portion of energy that has been diffusely reflected. The way the model is formulated allows for a dynamic control of the image source production, so that no fixed maximum order is required.

1 MODELS BASED ON GEOMETRICAL ACOUSTICS

Geometrical acoustics models are widely used in the study of sound fields in rooms, because they provide low cost predictions for complicated cases, such as theaters, concert halls, etc. In these models various wave phenomena degenerate to simple geometrical tasks. Furthermore, in most of them only the propagation of acoustical energy is considered, any phase information being neglected. For years, the most common room acoustic models, ray/beam tracing[1,2] and image source model (ISM),[3] were based on purely specular reflections. On the other hand, a less used method, acoustical radiosity (AR),[4,5] is based on purely diffuse reflections, represented by *Lambert's scattering law*.[4] In reality, neither purely diffuse nor purely specular reflections occur in rooms. Indeed the reflection on a real wall seems to be a mixture of these two extremes, and several authors have presented hybrid models in this direction. In 1993, Lewers[6] proposed a combination of beam tracing and AR. In 1996, Dalenbäck[7] proposed a cone tracing method that accounts for the diffuse reflection by the notion of *secondary sources*. In this paper a combination of AR and ISM is proposed for

[1]email: gk@odeon.dk
[2]email: jbr@elektro.dtu.dk
[3]email: chj@elektro.dtu.dk
[4]email: fja@elektro.dtu.dk

general polyhedral room cases. The new model is developed for energy impulse response predictions. Initially, the principles of the two methods are presented and afterwards ISM is merged into the AR equations, resulting in the formulation of the proposed model. In the complete version ISM and AR are coupled in both directions, where ISM is converted to AR and vise versa. A simplification is proposed so that only the conversion of ISM to AR is taken into account.

2 THEORETICAL BACKGROUND

2.1 Acoustic Radiosity

The initial formulation of the method was performed by Kuttruff in the early 1970s[4] and Miles[8] applied it for a rectangular room. The governing equation needs to be solved numerically, which involves discretization of the boundary into elements. The calculation of the response using AR is usually implemented in two parts. In the first part the energy history is computed for each element. This energy is a combination of the direct sound from the source and the interactions with the other elements due to diffuse reflections. Afterwards, the response at the receiver is calculated by collecting the contributions from the elements. Following the computer graphics approach, the first part is called *rendering* and the second part *gathering*.

The rate of energy that leaves a unit area of surface is defined as *radiation density* $B(t)$. It has the same unit as intensity but it is a scalar quantity, described in detail by Nosal *et al.*[5] The discretized form of the main AR equation reads:

$$B_i(t) = \rho_i \sum_{j=1}^{N} B_j \left(t - \frac{R_{i,j}}{c} \right) F_{i,j} e^{-\alpha_m R_{i,j}} + B_{i,Q}(t), \tag{1}$$

where the radiation density of the element i is obtained by the contributions of all other elements on the boundary in addition to the direct contribution $B_{i,Q}(t)$ from the source Q. The reflection coefficient ρ_i accounts for the portion of energy that is radiated by element i. The absorbed energy is represented by the absorption coefficient $\alpha_i = 1 - \rho_i$. In Eqn. (1) the exponential factor represents the air absorption, where α_m is the air absorption exponent. $R_{i,j}$ is the distance between the centroids of elements i and j and c is the sound speed. The term in the brackets represents the time delay involved between i and j. $F_{i,j}$ is the so called *form factor*,[9] which defines the fraction of energy that leaves element i and is received by element j, according to Lambert's law:

$$F_{i,j} = \frac{1}{S_i} \int_{S_i} \int_{S_j} \frac{\cos\theta \cos\theta'}{\pi R_{i,j}^2} \mathrm{d}S' \mathrm{d}S. \tag{2}$$

Here θ and θ' define the angles formed between the line connecting the centroids of the elements i, j and the corresponding normal vectors. Normally Eqn. (2) has to be evaluated numerically.

The direct contribution from the source to element i is

$$B_{i,Q}(t) = \frac{\rho_i}{4\pi S_i} W_Q \left(t - \frac{R_{i,Q}}{c} \right) H_{i,Q} e^{-\alpha_m R_{i,Q}}, \tag{3}$$

where W_Q is the power of the source, $R_{i,Q}$ is the distance between the element and the source, and $H_{i,Q}$ is the integral over the solid angle subtended by the element at the source:

$$H_{i,Q} = \int_{S_i} \frac{\cos\theta_Q}{R_{i,Q}^2} \, \mathrm{d}S. \tag{4}$$

In this paper all the integrals over solid angles are computed by a fast and accurate method, the *spherical triangle*, proposed by Nosal *et al.*[5] So far, it has been implied that when an element acts

as a source it is named j, while when it acts as a receiver it is named i. This convention is followed in the whole article.

Once every $B_i(t)$ has been calculated, the energy density at the receiver can be found by

$$E(t) = \frac{1}{\pi c}\sum_{j=1}^{N} B_j\left(t - \frac{R_{P,j}}{c}\right) H_{P,j} e^{-\alpha_m R_{P,j}} + E_Q(t), \quad H_{P,j} = \int_{S_i} \frac{\cos\theta_P}{R_{P,j}^2}\,\mathrm{d}S \tag{5}$$

is the integral over the solid angle subtended by the element j at the receiver P. $E_Q(t)$ is the direct contribution from the source, given by

$$E_Q(t) = \frac{1}{4\pi c R_{P,Q}^2} W_Q\left(t - \frac{R_{P,Q}}{c}\right) e^{-\alpha_m R_{P,Q}}. \tag{6}$$

2.2 Image Source Model

In ISM the energy is assumed to be reflected purely specularly. The reflection is modeled by mirroring the source behind the corresponding wall.[3] This leads to an *image source* q, whose contribution to the receiver is identical to the reflection from the wall. The first mirroring of the original source Q gives a first order reflection. Further mirroring of the image source behind another wall gives a higher order reflection. It is convenient to call every new image source as *daughter source* and its predecessor as *mother source*. Every time a source is mirrored back from a wall, its power is attenuated by the reflection coefficient of the wall, ρ. In an image source sequence, the power of the last image source has been attenuated by the product of all reflection coefficients of the precedent reflections. This product is called the *source factor*.

The general case of an arbitrary polyhedral room ISM proves to be very time consuming for typical impulse response lengths. The number of image sources follows an exponential growth with increasing order. Moreover, only a small part from the ensemble of image sources corresponds to feasible reflection paths and contributes to the impulse response.[10] Therefore, the most time consuming task in the general ISM is to filter out all the unwanted image sources.

3 COMBINED MODEL

The reflected energy is now further separated to a diffuse part, described by the *scattering coefficient* s and a specular part, $(1-s)$. As a result, the diffuse reflection coefficient is $s(1-\alpha)$ while the specular is $(1-s)(1-\alpha)$. Conservation of energy implies that

$$\alpha + s(1-\alpha) + (1-s)(1-\alpha) = 1. \tag{7}$$

3.1 Image Sources

The idea now is to represent all the specular refections from the original source by its image sources up to order λ. If l denotes the intermediate reflections up to λ, then each reflecting wall can be represented by w_l, taking values from 1 to the total number of walls N_w in the room. With this nomenclature, the source factor of an image source q_k is

$$r_{q_k} = \prod_{l=0}^{\lambda} (1 - s_{w_l})\rho_{w_l}. \tag{8}$$

The special product $(1-s_{w_0})\rho_{w_0} = 1$ symbolizes the direct contribution, so that the original source, Q has a source factor of 1. The subindex $k = 1, 2, \ldots$ denotes the numbering of the image source. When $k = 0$, define $q_0 \equiv Q$. The purely specular energy density reaching any receiver P in the

room is computed as the sum of the contributions from all effective image sources and the direct contribution:

$$E_{q_k}(t) = \frac{1}{4\pi c} \sum_{k=0}^{\infty} \frac{r_{q_k}}{R_{P,q_k}^2} W_Q \left(q_k, t - \frac{R_{P,q_k}}{c} \right) e^{-a_m R_{P,q_k}}. \tag{9}$$

The boundary of the room is subdivided into elements, in order to represent the diffuse reflections. Each of the elements acts as a new receiver of specular reflected energy from the image sources. The specular component of the radiation density for each element, together with the direct contribution from the image sources, is

$$B_{i,q_k}(t) = \frac{s_i \rho_i}{4\pi S_i} \sum_{k=0}^{\infty} r_{q_k} W_Q \left(q_k, t - \frac{R_{i,q_k}}{c} \right) H_{i,q_k} e^{-a_m R_{i,q_k}}, \tag{10}$$

where S_i is the area of the element, R_{i,q_k} is the distance between the image source and the element, and

$$H_{i,q_k} = \int_{S_i} \frac{\cos\theta_{q_k}}{R_{i,q_k}^2} \, \mathrm{d}S \tag{11}$$

is the integral over the solid angle subtended by the element at the source.

3.2 Image Elements

The diffuse energy reflected by an element on the boundary is free to be reflected afterwards either diffusely again or specularly. The first case is already represented by AR and the other elements on the boundary. The second case can be modeled by the notion of image elements, similar to the image sources of the original source. The principle is illustrated in Fig. 1, where the mirroring of the source element behind the wall gives the full path of the first order reflection at the receiving element.

For every element j a sequence of image elements is generated. Similar to the image sources, the index m is used to number these image elements. Therefore, a specific image element associated with the element j is denoted by the subindex jm. The radiation density of each image element is the same as that of the source element, attenuated by the corresponding source factor,

$$r_{jm} = \prod_{l=0}^{\lambda} (1 - s_{w_{jl}}) \rho_{w_{jl}}, \tag{12}$$

similar to Eqn. (8), where λ indicates the reflection order of jm and jl is the indexing of the mirroring walls involved in the generation of jm. As before, the product $(1 - s_{w_{j0}})\rho_{w_{j0}} = 1$ corresponds to the direct contribution from the source element j. The energy transfer from an image element jm to a receiving element i can be implemented by generalizing the classical form factor of Eqn. (2) for any pair of elements, image or real:

$$F_{i,jm} = \frac{1}{S_i} \int_{S_i} \int_{S_{jm}} \frac{\cos\theta \cos\theta''}{\pi R_{i,jm}^2} \, \mathrm{d}S'' \, \mathrm{d}S. \tag{13}$$

This new form factor is called *extended form factor*. Apparently, $S_{jm} = S_j$. For optimizing purposes it can be assumed that the energy does not vary over i so that Eqn. (13) is simplified to

$$F_{i,jm} \approx \int_{S_{jm}} \frac{\cos\theta \cos\theta''}{\pi R_{i,jm}^2} \, \mathrm{d}S''. \tag{14}$$

This simplification can be justified by the fact that with increasing order the image elements are placed further and further away from i, so that the *five times rule* from computer graphics can be applied.[9]

3.3 Formulation of the Proposed Model

Equation (1) can now be extended to include the specular components by the image sources and the image elements. The radiation density of the receiving element i becomes

$$B_i(t) = s_i\rho_i \sum_{j=1}^{N}\sum_{m=0}^{\infty} r_{jm}B_j\left(t - \frac{R_{i,jm}}{c}\right)F_{i,jm}e^{-a_m R_{i,jm}} + B_{i,q_k}(t). \tag{15}$$

The first double summation represents the contribution from all source elements and their images. The first term of the inner summation (for $m = 0$) is identical to the first term in Eqn. (1), corresponding to the direct contribution from j to i. In the extended AR equation the scattering coefficient has been used, indicating that only a fraction s_i of the reflected energy is diffusely reflected from i in contrast to Eqn. (1). The second term is the specular contribution from Q, given by Eqn. (10).

The energy density at the receiver can be calculated by extending Eqn. (5) in the same way as for Eqn. (15):

$$E(t) = \frac{1}{\pi c}\sum_{j=1}^{N}\sum_{m=0}^{\infty} r_{jm}B_j\left(t - \frac{R_{P,jm}}{c}\right)H_{P,jm}e^{-a_m R_{P,jm}} + E_{q_k}(t). \tag{16}$$

Again, the first double summation corresponds to the contribution from all elements (source and image), that is from all specular reflections of the diffuse energy that reach the receiver. The second term is the specular contribution from Q, given by Eqn. (9).

At this point it seems impractical to include all the orders of reflection for the usual impulse response lengths. The computation time would raise abruptly and the information gained would be useless because the energy at the late part of the response would be already diffuse. Thus, it seems wise to use both ISM and AR for the early part of the response but only AR for the late part. The number of image sources can be finite, K, corresponding to the first few reflection orders. The energy contribution from the last image source K is reflected totally in a diffuse manner at element i, since no further specular reflections are assumed. Figure 2 illustrates two unique specular reflection paths and their conversion to totally diffuse ones. The upper one represents a sequence of image sources while the lower one represents a sequence of image elements. During the final reflection the energy is assumed only diffusely reflected. Eqn. (15) is now modified as

$$\begin{aligned} B_i(t) \simeq \sum_{j=1}^{N}\Bigg[& s_i\rho_i \sum_{m=0}^{M-1} r_{jm}B_j\left(t - \frac{R_{i,jm}}{c}\right)F_{i,jm}e^{-a_m R_{i,jm}} \\ & + \rho_i r_{jM}B_j\left(t - \frac{R_{i,jM}}{c}\right)F_{i,jM}e^{-a_M R_{i,jM}}\Bigg] + B_{i,q_k}(t), \end{aligned} \tag{17}$$

where

$$\begin{aligned} B_{i,q_k}(t) \simeq & \frac{s_i\rho_i}{4\pi S_i}\sum_{k=0}^{K-1} r_{q_k}W_Q\left(q_k, t - \frac{R_{i,q_k}}{c}\right)H_{i,q_k}e^{-a_m R_{i,q_k}} \\ & + \frac{\rho_i}{4\pi S_i}r_{q_K}W_Q\left(q_K, t - \frac{R_{i,q_K}}{c}\right)H_{i,q_K}e^{-a_m R_{i,q_K}}. \end{aligned} \tag{18}$$

Secondly, the double summation in Eqns. (15) and (16) is the most computationally costly term, when implementing combined model. A question arises now whether the role of image elements is really important or not. It may be argued that once the energy is diffusely reflected any subsequent specular reflections can be judged as diffuse anyway. In that case, the two primitive models, ISM and AR, can be considered as coupled only towards one direction, from ISM to AR. As a result, Eqns. (15) and (16) are simplified to

$$B_i(t) \simeq \rho_i \sum_{j=1}^{N} B_j\left(t - \frac{R_{i,j}}{c}\right)F_{i,j}e^{-a_m R_{i,j}} + B_{i,q_k}(t), \tag{19}$$

$$E(t) \simeq \frac{1}{\pi c} \sum_{j=1}^{N} B_j \left(t - \frac{R_{P,j}}{c} \right) H_{P,j} e^{-a_m R_{P,j}} + E_{q_k}(t). \tag{20}$$

So now the energy from the source element j is reflected only diffusely at element i and the total reflection coefficient ρ_i is used. The validity of this simplification will be examined in Sec. 5.

4 IMPLEMENTATION OF THE MODEL

For the implementation of the model an impulsive original source is assumed, i.e., $W_Q = 1$ for $t = 0$ and $W_Q = 0$ for $t \neq 0$. Therefore, Eqn. (18) is normalized with W_Q. Moreover, the air absorption can be fully neglected until the final step of the calculations. Once the energy density at the receiver has been computed without air absorption – let us call it $E_0(t)$ – the corrected value is given by:

$$E_{a_m}(t) = E_0(t) e^{-a_m t c}. \tag{21}$$

The time is discretized by a sampling frequency f_s. Each time step is now denoted by an integer n, so that the actual time at n is $t_n = n\,\mathrm{d}t$. Now, $t = 0$ is represented by $n = 1$. Evidently, the higher the sampling frequency the more accurate the response is, but the computation time becomes longer. A compromise between the duration of the response, the accuracy desired and the computation time allowed should lead to an optimal selection of f_s. Following Nosal *et al.*,[5] all the delays between the elements, the source and the receiver can be expressed by a number of time steps, utilizing the ceiling function ($\lceil \cdot \rceil$). For example, the delay between i and j is expressed as $T_{i,j} = \lceil R_{i,j}/(c\,\mathrm{d}t) \rceil$. Similarly, the length of the discretized impulse response is $T = \lceil t_{max}/\,\mathrm{d}t \rceil$, where t_{max} is the actual duration.

4.1 The Main Algorithm

The model is implemented in an iterative algorithm, where each iteration is equivalent to the order of reflection. A central feature is the *radiation response* of each element i, describing the whole time vector of the radiation density associated with it. This is symbolized by $B[i, 1:T]$. Similar to the radiation response, the *receiver's response* is denoted by $E[1:T]$. These vectors essentially represent the reflectograms, with respect to the impulsive source. During each iteration the whole vectors are updated, so that they become more dense and longer, occupying progressively a larger part of the desired total duration. This can been seen as a convergence towards a final solution, where the receiver's response $E[1:T]$ has been stabilized and it does not change with further iterations.

Initially, the simplified version of the model is considered, as given by Eqns. (19) and (20). The corresponding algorithm is called *main algorithm*. In Sec. 4.3 the complete problem is treated as given by Eqns. (15) and (16). During the primary iteration the direct contribution from the original source to the elements and the receiver is calculated. In addition, the first order image sources are generated for any semi-diffuse surface. At the end of the primary iteration each $B[i, 1:T]$ and $E[1:T]$ contain only one bin corresponding to the impulse from the source. In the next iteration every element collects the radiation response from all other elements, updating its old radiation response. The corresponding assignment for every pair i and j reads

$$B[i, T_{i,j}+1:T] \coloneqq B[i, T_{i,j}+1:T] + \beta_i B\,[j, T - T_{i,j}]\, F_{i,j}, \tag{22}$$

where $\beta_i = \rho_i$, because the energy from j is assumed to be reflected totally diffusely at i. The symbol $\coloneqq$ implies that a new value is assigned to the old value of the variable. Once the source element has distributed all of its present energy, $B[j, 1:T]$ is reset to zero. In the same way to Eqn. (22) the receiver gathers energy from each element according to

$$E[T_{P,j}+1:T] \coloneqq E[T_{P,j}+1:T] + \frac{1}{\pi c} B\,[\,j, 1:T - T_{P,j}]\,. \tag{23}$$

Equations (22) and (23) essentially represent the diffuse model for the first order reflection. As for the specular model, all first order image sources are processed one after the other. For each source the receiver is checked whether it is visible. If so, the contribution is added:

$$E_q[T_{P,q_k}] := E_q[T_{P,q_k}] + \frac{1}{4\pi c}\frac{r_{q_k}}{R^2_{P,q_k}}. \tag{24}$$

Now, all walls are processed in a loop that serves two purposes: 1) The energy contribution from the image source is computed for all visible elements on each wall. For simplicity, only the center of the element is taken into account for the visibility check. 2) The valid daughter image sources are generated.

According to the assumption of Eqn. (18), the incident energy from the image source is reflected by a portion $s_i\rho_i$ from element i, as long as the source produces a daughter source behind the wall of i. If it is not the case, the corresponding specular reflection path is terminated and the portion is ρ_i. Compactly, the contribution from the image source reads

$$B[i, T_{i,q_k}] := B[i, T_{i,q_k}] + \beta_i \frac{1}{4\pi S_i} r_{q_k} H_{i,q_k}, \tag{25}$$

where $\beta_i = \rho_i$, if the source is the last one and $\beta_i = s_i\rho_i$, otherwise. At the end of the first order iteration, the diffuse and specular contributions have updated the radiation and the receiver's responses. Every successive iteration can be executed with the same procedure, with the image and secondary sources contributing the corresponding order of specular and diffuse reflection, respectively.

4.2 Dynamic Termination of the Image Source Sequence

The upper limit of the summation in Eqn. (18) can be predefined by fixing the maximum order of image sources, like in the pure ISM. However, surfaces with high scattering coefficient are expected to reflect only a small portion of energy in a specular manner. In such cases, the corresponding image sources are very weak. Furthermore, as more and more specular rays become diffuse during each iteration, the energy in the specular model is expected to decrease, raising the energy in the diffuse model. Consequently, it would be wise to convert the combined model dynamically to pure AR, whenever the diffuse model dominates the specular, accelerating the computational effort.

For that reason the diffuse and specular radiation densities of a wall can be defined, denoted by B_{dw} and B_{sw}, respectively. The first one represents the energy of the wall in the diffuse model – without adding the contribution from the image sources. The second one contains only the specular contribution. Every time a daughter source is to be produced behind a wall w, the specular radiation density arriving at the wall from the mother source q_k at time step T_{w,q_k} is compared with the diffuse radiation density at the same time step. If $B_{sw} > B_{dw}[w, T_{w,q_k}]$, the daughter source is produced behind the wall, because the energy in the specular model is still important, compared to the energy in the diffuse one. On the other hand, if $B_{sw} < B_{dw}[w, T_{w,q_k}]$ the image source sequence is terminated. The termination condition can be subjected to a predefined margin. Someone could demand, for example, that it is enough for the specular energy to be higher than 50% of the diffuse energy, in order for the image source sequence to be continued. The lower the margin is, the later the image source sequence is terminated.

4.3 The Full Algorithm

Now the complete coupling between AR and ISM is included, by letting the energy emitted from the elements suffer several specular reflections while it is distributed on the boundary. According to Sec. 3, these specular reflections are represented by image elements. Now $\beta_i = s_i\rho_i$ in Eqn. (22). In order to simplify the algorithm, the termination order for the image elements is fixed. The reflection

orders of the image elements can work independently of the orders/iterations of the main algorithm. This allows to set a relative low number of reflections for the image elements, in order to keep the computational cost as low as possible.

4.4 Impulse Response Due to the Image Elements

During each iteration a new ensemble of image elements is formed for every source element j, representing the lower path in Fig. 2. However, the way all the image elements of j contribute at element i is a matter of geometry and remains the same for all iterations. Thus, there is no need to generate them from scratch. It is enough to store the radiation response of each element i due to the image elements of j, when it emits a unit impulse ($B[j,0] = 1$):

$$B_m[i,j,T_{i,jm}] := B_m[i,j,T_{i,jm}] + s_i\rho_i \sum_{m=1}^{M-1} r_{jm}F_{i,jm} + \rho_i r_{jM}F_{i,jM}. \tag{26}$$

Discrete convolution of $B_m[i,j,n]$ with the real $B\,[\,j,n]$, gives the real radiation density as a function of time:

$$B[i,n] := B[i,n] + B_m[i,j,n] * B\,[\,j,n] := B[i,n] + \sum_{\tau=n}^{T} B_m[i,j,\tau]\cdot B\,[\,j,\tau-n+1]\,. \tag{27}$$

Equation (26) leads to a three dimensional (3D) matrix: for every source element j, every receiving element i and every time step n. 3D matrices are very impractical and difficult to be stored. Transformation into two dimensional (2D) is quite beneficial. For that reason a very low sampling frequency could be adopted only for the $B_m[i,j,1:T]$. Hence, the responses due to the image elements will be a bit coarse but this does not seem to harm the result. The important thing is that many reflections can be grouped into one bin, as long as they arrive at the same time interval. Then it seems useful to store only the bins and their arrival times, not the whole time vectors $B_m[i,j,1:T]$, which contain usually a large number of zeros among the bins. Hence two 2D matrices should be created; one for the values of $B_m[i,j,1:T]$ and one for the corresponding arrival time steps. Their columns represent the receivers i, while the lines are divided into groups of source elements j. In each group, every line corresponds to one bin of the response.

Following the same process, the receiver's response due to the image elements of j can be computed when the element acts as a unit impulse source:

$$E_m[\,j,T_{P,jm}] := E_m[\,j,T_{P,jm}] + \frac{1}{\pi c}\sum_{m=1}^{M} r_{jm}H_{P,jm}. \tag{28}$$

The result can be stored directly in a 2D matrix with j lines and n columns. Then the real energy density, $E[n]$, due to the image elements of j, can be computed by discrete convolution with $B\,[j,n]$:

$$E[n] := E[n] + E_m[\,j,n] * B\,[\,j,n] := E[n] + \sum_{\tau=n}^{T} E_m[\,j,\tau]\cdot B\,[\,j,\tau-n+1]\,. \tag{29}$$

5 RESULTS AND ANALYSIS

5.1 A Polyhedral Room with Varying Scattering

A small polyhedral room of 7 walls – Fig. 3(a) – was studied. The boundary was subdivided into 276 elements and a sampling frequency of 16 kHz was used. The sampling frequency was chosen relatively low in order to help for better visibility of the reflectograms. The absorption and scattering coefficients of the walls are given in Table 1. In the first case the scattering coefficient

was everywhere 1, meaning that the pure AR algorithm was used in the calculations. In the second case the scattering coefficient varied significantly and the combined model was employed. The reflectograms at the receiver for both cases are given in Fig. 3(b). The line corresponding to AR is very smooth throughout the whole impulse response length. The early reflections have lost all of their specular nature. On the other hand, the reflectogram by the combined model preserves a lot of information for the specular reflections in the early part (highly oscillating behavior) and converges smoothly to the straight AR line only at the late part, as the specular reflections are gradually converted to diffuse ones.

5.2 Prediction of Flutter Echo

One interesting application of the main algorithm is the prediction of flutter echoes, which are difficult to simulate properly by the existing room acoustic methods. A rectangular room was considered with dimensions $(L_x, L_y, L_z) = (8, 5, 3)$ m and coefficients from Table 2. The absorption and scattering was quite low for two parallel lateral walls, while it was high for the rest. The boundary was subdivided into 252 elements and the sampling frequency was 2.7 kHz. The source was placed at the center of the room, $Q = (4, 2.5, 1.5)$ m, and the receiver was placed between the source and one of the specular reflecting walls, $P = (4, 1.25, 1.5)$ m. The simulation was run with 7 iterations. After the first iteration all the weak image sources had been aborted. Then, only two image sources were produced per iteration, corresponding to the pair of the specular parallel walls.

The reflectogram at the receiver is illustrated in Fig. 4(a). There are 14 equally spaced prominent bins, just after the direct contribution. These bins form 7 pairs, corresponding to the number of iterations used in the simulation. The advantage of the combined model in the case of highly symmetrical problems, like flutter echo, is that the computational load is mitigated by the fact that only the important image source sequences are kept, while the rest of the problem is handled by the much faster AR part. Figure 4(b) gives a global picture of the energy behavior in the room. The energy received by each element at every time step was calculated first. Then the averaged energy from all the elements at every time step was computed. By backward integration the energy decay curves were obtained. The individual decay curves from 22 random elements are given by the thin lines. The bold line is the decay curve of the averaged energy. Evidently, the curves corresponding to the elements on the parallel specular walls have shallower slope and they are elevated above the average. The energy decay at these elements reveals the repeatable reflections of the flutter echo and leads to a decrease of the slope at the late part of the average energy.

5.3 Computational Performance

The reflections in AR are memoryless, so that the execution time of the method remains stable as the order of reflection is increased, in contrast to ISM. As for the execution time of the combined model, this highly depends on which of the two methods is dominant for each reflection level. During the early reflections ISM carries most of the information, so that the computational effort per reflection order is increased. As the specular reflections are converted to diffuse, AR is dominant and the computational effort is stabilized.

In the following example, the room of Sec. 5.1 was used with the absorption data for case 2 in Table 1. The combined model was run with the scattering coefficient varying uniformly from 0 to 1. In total, 18 iterations were performed with a sampling frequency of 20 kHz. The duration of the impulse response was 35 ms. A dynamic termination of image sources was used (Sec. 4.2). The Cpu time for execution was recorded for every iteration and the result is illustrated in Fig. 5. The execution time is proportional to the number of generated image sources. For pure specular reflections it increases monotonically. Applying $s = 0.1$ to all walls is enough to introduce a “peak"

in the computational time, after which it declines gradually. For s = 0.2 the execution time has been dramatically reduced and for $s > 0.4$ it is almost the same as with $s = 1$ (pure AR).

6 CONCLUSIONS

An attempt to combine AR and ISM has been presented in order to model the mixed kind of specular and diffuse reflections observed on real walls, inside rooms. The combined model utilizes the most efficient parts of the two methods and makes it feasible to use ISM up to very high order, preserving at the same time the important specular information missed by AR. As a result, interesting phenomena like flutter echoes can be simulated precisely, with low cost. In general, the model serves for a unified predictor of both the early and the late part of the response. Unlike other room acoustic models that incorporate specular and diffuse reflections by a tracing process, the presented one is fully deterministic, providing high detail and reproducibility of the results.

7 REFERENCES

[1] A. Krokstad, S. Strøm, and S. Sørsdal, "Calculating the acoustical room response by the use of a ray tracing technique.", J. Sound Vib. **8**, 118–125 (1968).

[2] C.-H. Jeong, J.-G. Ih, and J. H. Rindel, "An approximate treatment of reflection coefficient in the phased beam tracing method for the simulation of enclosed sound fields at medium frequencies", Appl. Acoust. **69**, 601–613 (2008).

[3] J. Borish, "Extension of the image model to arbitrary polyhedra", J. Acoust. Soc. Am. **75**, 1827–1836 (1984).

[4] H. Kuttruff, *Room Acoustics,* 4th ed. (Applied Science Publishers LTD, London, 2000), Chap. 4, pp. 110-114.

[5] E. M. Nosal, M. Hodgson, and I. Ashdown, "Improved algorithms and methods for room sound-field prediction by acoustical radiosity in arbitrary polyhedral rooms", J. Acoust. Soc. Am. **116**, 970–980 (2004).

[6] T. Lewers, "A combined beam tracing and radiant exchange computer model of room acoustics", Appl. Acoust. **38**, 161–178 (1993).

[7] B. I. Dalenbäck, "Room acoustic prediction based on a unified treatment of diffuse and specular reflection.", J. Acoust. Soc. Am. **100**, 899–909 (1996).

[8] R. N. Miles, "Sound field in a rectangular enclosure with diffusely reflecting boundaries", J. Sound Vib. **92**, 203–226 (1984).

[9] I. Ashdown, *Radiosity: A Programmer's Perspective,* 1st ed. (Wiley, New York, 1994), Chap. 2, pp. 46-53 and Chap. 5, pp.277-278.

[10] M. Vorländer, "Simulation of the transient and steady state sound propagation in rooms using a new combined ray-tracing / image-source algorithm", J. Acoust. Soc. Am. **86**, 172–178 (1989).

[11] International Organization for Standardization, Geneva, Switzerland, *ISO 3382-1. Acoustics - Measurement of room acoustic parameters - Part 1: Performance spaces* (2009).

	Walls	1	2	3	4	5	6	7	
	S_w (m^2)	0.54	0.41	0.49	0.65	0.34	0.54	0.65	
	α	0.8	0.3	0.7	0.1	0.0	0.2	0.6	$\bar{\alpha}$ = 0.40
case 1	s	1.0	1.0	1.0	1.0	1.0	1.0	1.0	$\bar{s}$ = 1.00
case 2	s	0.6	0.0	0.2	0.2	0.0	0.1	0.4	$\bar{s}$ = 0.24

Table 1: *Absorption and scattering coefficients for the two cases in Sec. 5.1 – averaged values are shown on the left.*

Walls	1	2	3	4	5	6	
S_w (m^2)	40.0	40.0	15.0	15.0	24.0	24.0	
α	0.8	0.8	0.8	0.8	0.2	0.2	$\bar{\alpha}$ = 0.62
s	1.0	1.0	1.0	1.0	0.0	0.0	$\bar{s}$ = 0.70

Table 2: *Absorption and scattering coefficients for investigation of flutter echo in the rectangular room – averaged values are shown on the left.*

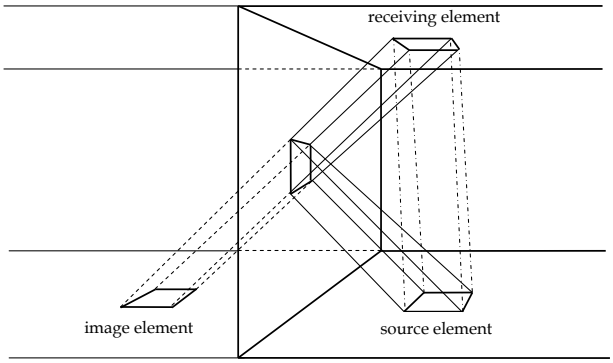

Figure 1: *The diffusely reflected energy from the source element can reach the receiving element either directly (–·–·–) or via a specular reflection (– – –), represented by the image element.*

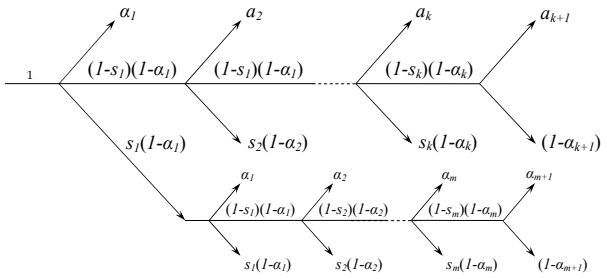

Figure 2: *Flow of energy in two reflection paths. The upper path represents a single image source sequence for the original source. The lower path represents a single image element sequence for one of the elements acting as a source. When any of the paths is terminated, the specular coefficient,* $(1 - s)$*, becomes zero and from now on, the energy is reflected totally diffusely.*

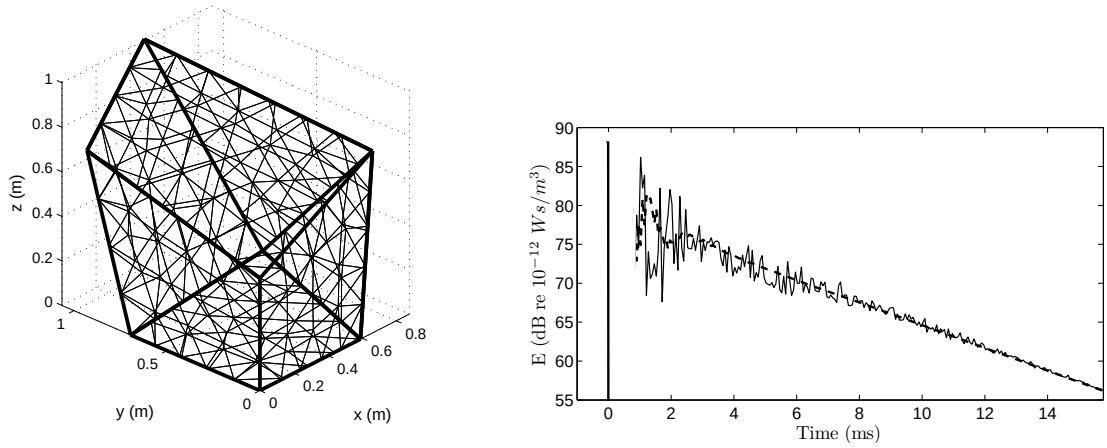

(a) (b)

Figure 3: (a): *A 7-wall polyhedral room meshed with N=276 triangular elements. Source:* $Q = (0.3, 0.2, 0.2)$ *m. Receiver:* $P = (0.4, 0.7, 0.5)$ *m.*. (b): *Reflectograms at the receiver in the room. Coefficients from Table 1.* – – –*: Case 1.* ——*: Case 2.*

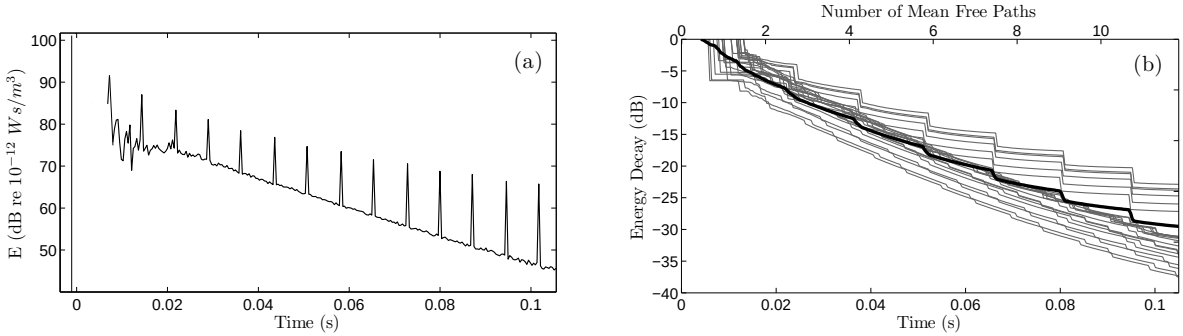

Figure 4: *Demonstration of flutter echo. Results obtained by the combined model with coefficients from Table 2.* (a) *Reflectogram at the receiver.* (b) ——*: Individual decay curves from 22 uniformly chosen elements,* ——*: Decay curve of averaged energy.*

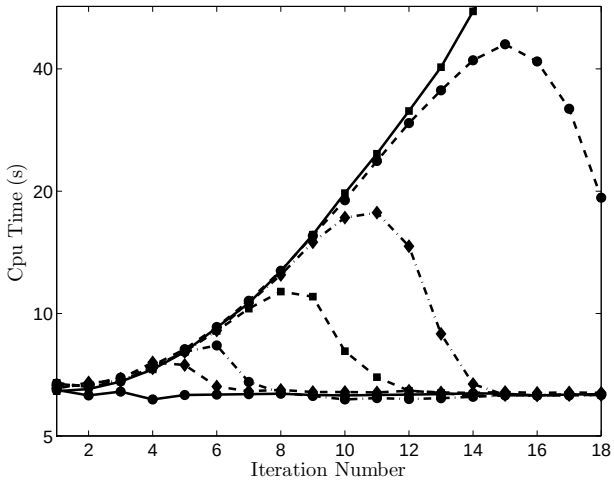

Figure 5: *Execution time per iteration for different uniform scattering coefficients.* —■—*:* $s = 0$, - -●- - *:* $s = 0.1$, -·◆·- *:* $s = 0.15$, - -■- - *:* $s = 0.2$, -·●·- *:* $s = 0.3$, - -◆- - *:* $s = 0.4$, —●—*:* $s = 1$.